ACS chemical biology

Articles

pubs.acs.org/acschemicalbiology

Api88 Is a Novel Antibacterial Designer Peptide To Treat Systemic Infections with Multidrug-Resistant Gram-Negative Pathogens

Patricia Czihal,[†,‡] Daniel Knappe,[†,‡] Stefanie Fritsche,[‡,§] Michael Zahn,[†,‡] Nicole Berthold,[†,‡] Stefania Piantavigna,[∥] Uwe Müller,[‡,§] Sylvia Van Dorpe,[⊥] Nicole Herth,[†,‡] Annegret Binas,[¶] Gabriele Köhler,[+] Bart De Spiegeleer,[⊥] Lisandra L. Martin,[∥] Oliver Nolte,[¶] Norbert Sträter,[†,‡] Gottfried Alber,[‡,§] and Ralf Hoffmann*[,†,‡]

[†]Institute of Bioanalytical Chemistry, Faculty of Chemistry and Mineralogy, [‡]Center for Biotechnology and Biomedicine, and [§]Institute of Immunology, College of Veterinary Medicine, Universität Leipzig, Leipzig, Germany

[∥]School of Chemistry, Monash University, Clayton, Victoria, Australia

[⊥]Drug Quality and Registration (DruQuaR) Group, Faculty of Pharmaceutical Sciences, Ghent University, Ghent, Belgium

[¶]AiCuris GmbH & Co KG, Building 302, Wuppertal, Germany

[+]Institute of Pathology, University Hospital Münster, Münster, Germany

Supporting Information

ABSTRACT: The emergence of multiple-drug-resistant (MDR) bacterial pathogens in hospitals (nosocomial infections) presents a global threat of growing importance, especially for Gram-negative bacteria with extended spectrum β-lactamase (ESBL) or the novel New Delhi metallo-β-lactamase 1 (NDM-1) resistance. Starting from the antibacterial peptide apidaecin 1b, we have optimized the sequence to treat systemic infections with the most threatening human pathogens, such as *Escherichia coli*, *Klebsiella pneumoniae*, *Pseudomonas aeruginosa*, and *Acinetobacter baumannii*. The lead compound Api88 enters bacteria without lytic effects at the membrane and inhibits chaperone DnaK at the substrate binding domain with a K_D of 5 μmol/L. The Api88-DnaK crystal structure revealed that Api88 binds with a seven residue long sequence (PVYIPRP), in two different modes. Mice did not show any sign of toxicity when Api88 was injected four times intraperitoneally at a dose of 40 mg/kg body weight (BW) within 24 h, whereas three injections of 1.25 mg/kg BW and 5 mg/kg BW were sufficient to rescue all animals in lethal sepsis models using pathogenic *E. coli* strains ATCC 25922 and Neumann, respectively. Radioactive labeling showed that Api88 enters all organs investigated including the brain and is cleared through both the liver and kidneys at similar rates. In conclusion, Api88 is a novel, highly promising, 18-residue peptide lead compound with favorable *in vitro* and *in vivo* properties including a promising safety margin.

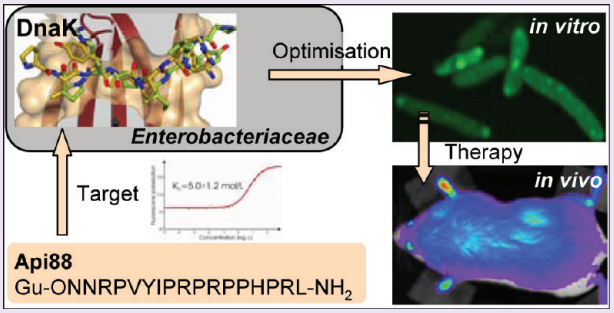

The discovery and subsequent use of antibiotics more than 60 years ago has revolutionized the treatment of previously deadly infections and thus dramatically reduced the rate of mortality and morbidity of infectious diseases. During the golden age of antibiotics the Surgeon General of the USA declared "It is time to close the book on infectious disease"; this was in 1967.[1] More recently, in 1998 the new Surgeon General stated that "infectious disease are a rising peril". Today bacterial infections are still the leading cause of death worldwide, with antibiotic resistance being one of the greatest pharmaceutical challenges. Despite recent evidence that indicates bacterial resistance is an ancient phenomenon, genetically encoded in 30,000-year-old bacterial DNA samples,[2] the continuous and selective antibiotic pressure has produced resistant pathogens[3] over recent decades. Currently, Gram-negative bacteria are causing increasing concern due to the rapid spread of multi- or even pan-resistant strains, *e.g.*, the NDM-1 carbapenemase producing Enterobacteriaceae.[4,5] While many isolates of Gram-negative bacteria respond well to antimicrobial treatments, the sudden emergence and rapid spread of an unprecedented resistance problem highlights the desperate need for novel antibiotics to combat the most threatening Enterobacteriaceae (*Escherichia coli*, *Klebsiella pneumoniae*, and *Enterobacter cloacae*) and non-fermenting species (*Acinetobacter baumannii* and *Pseudomonas aeruginosa*).

Besides the challenge to circumvent these resistance mechanisms, certain pharmacodynamic requirements make drug development even more complex. While distribution in the bloodstream is readily achieved by i.v. infusion, sufficient drug concentrations in other target organs, and in particular the cerebrospinal fluid (CSF), are much more difficult to achieve.

Received: February 11, 2012
Accepted: May 2, 2012
Published: May 17, 2012

 © 2012 American Chemical Society

Table 1. Sequences of Native Apidaecin 1b and the Optimized Designer Peptides and Their MIC Values Determined in 1% TSB against Two *E. coli* and One *K. pneumoniae* strains

		MIC (μg/mL)		
code	sequence[a]	*E. coli* BL21 AI	*E. coli* D31[b]	*K. pneumoniae* K6[c]
1b	GNNRPVYIPQPRPPHPRL-OH	1	32	64
Api6	GNNRPVYIPQPRPPHPRL-NH_2	0.5	1	16
Api7	Ac-ONNRPVYIPQPRPPHPRL-NH_2	0.5	8	64
Api39	Ac-ONNRPVYIPRPRPPHPRL-NH_2	2	4	16
Api88	Gu-ONNRPVYIPRPRPPHPRL-NH_2	0.5	0.5	0.5

[a]Gu denotes *N,N,N′,N′*-tetramethylguanidine, and O denotes L-ornithine. [b]*E. coli* D31 is pathogenic with extended spectrum β-lactamase. [c]K6 is a pathogenic *K. pneumoniae* strain resistant against ampicillin, chloramphenicol, tetracyclin, *etc.*

Bacteria, in contrast, can traverse the blood-brain barrier (BBB) by several mechanisms and pathways or infect the central nervous system (CNS) during neurosurgical procedures. Some bacteria even produce molecules (*e.g.*, pneumolysin) that damage the BBB and will contribute to the entry of the bacteria into the CNS. Once inside the CNS, the pathogen triggers an inflammatory reaction that contributes to degradation of the BBB. Several pathogens, such as *E. coli*, group B *Streptococcus*, *Streptococcus pneumoniae*, *Listeria monocytogenes*, and *Neisseria meningitides*, were shown to enter the brain[6,7] relatively easily, causing neurological disorders. While the CNS may react to the infection, with microglia being key to the CNS immune defense cells,[8] this is quite often insufficient and leads to high morbidity and mortality.

Cationic gene-encoded host defense peptides (HDP) are nature's most diverse and most abundant class of antibiotics. All higher organisms produce these peptides as part of their innate immune system. A subset of the HDP, *i.e.*, antimicrobial peptides (AMP), possesses a direct antimicrobial activity by disruption of the bacterial membrane integrity and/or by translocation through the bacterial membranes. The mechanism for translocation often results in the inhibition of intracellular targets, such as DNA/RNA synthesis, protein synthesis/folding, cell wall synthesis, and cell division.[9] Thus AMP provide an ideal and novel series of lead compounds. Furthermore, they can be optimized for human applications, which appears especially promising for AMP inhibition of selective bacterial targets with little or no cross reactivity toward the human analogues. Short proline-rich AMP isolated from insects represent one promising class of compounds as they can be easily synthesized on solid phase, are relatively stable against proteases due to the high proline content, are nontoxic to human cell lines, and are predominantly active against Gram-negative bacteria including *E. coli*.[10] Among these, the family of apidaecins consists of more than 20 highly conserved peptides isolated from different lymph fluids of bees and wasps.[11] Apidaecins are 18−20 residues long and contain the highly conserved C-terminal sequence PRPPHPR(L/I), believed to be responsible for the translocation through the bacterial membrane.[12,13] The N-terminal domain appears to modulate the activity against different Gram-negative bacteria. Apidaecin 1b, which is the best studied apidaecin representative, is highly active against *E. coli*, less active against *K. pneumoniae*, and inactive against *P. aeruginosa*.[14] Although some recent reports indicate potential medical applications of apidaecins, it has not been optimized for systemic therapies or tested in animal models. Recent studies with longer proline-rich AMP (~40 residues), *i.e.*, A3-APO and Bac7, indicate a high *in vivo* efficacy in rodents, which was partially attributed to immunomodulatory effects.[15−17] Here, we report the rational design of a novel 18 residue peptide derivative starting from apidaecin 1b originally isolated from honey bees, which is active against the most threatening Gram-negative human pathogens, with very promising *in vitro* characteristics and high *in vivo* efficacy in two murine *E. coli* infection models.

RESULTS AND DISCUSSION

Improving the Activity and Expanding the Bacterial Spectrum. Apidaecin 1b was very effective against non-pathogenic *E. coli* BL21 AI (MIC 1 μg/mL), but much less active against the multiresistant strains *E. coli* D31 and *K. pneumoniae* K6 (MIC 32−64 μg/mL) (Table 1). Amidation of the C-terminus improved the activity 32- and 4-fold, respectively (Table 1, Api6). Acetylation of the N-terminus was designed to improve the protease stability; however, this abolished the activity against both strains indicating that an N-terminal positive charge is essential. Subsequent substitution of Gly^1 with ornithine or lysine restored the activity against *E. coli* (Api7). As trypsin-like proteases do not cleave peptide bonds that are C-terminal to an ornithine,[18] this amino acid was preferred over lysine to prevent degradation of the peptide by either human proteases (*e.g.*, serum proteases) or bacterial proteases. Another favorable substitution was replacement of the glutamine at position 10 with the basic residue arginine (Api39), which improved the activity against *K. pneumoniae* about 4-fold, although the activity against *E. coli* BL21AI was reduced by the same amount. This loss of activity against *E. coli* BL21AI appeared to be tolerable, as the dose required to treat systemic infections would be determined by the least accessible pathogen. In order to further increase the positive charge of the peptide, we replaced the N-terminal acetyl amide (CH_3CO-NH-) by *N,N,N′,N′*-tetramethylguanidine ($(((CH_3)_2N)_2$-C-NH-), which significantly reduced the MIC values to 0.5 μg/mL for both *E. coli* and *K. pneumoniae* strains (Table 1, Api88).

Thus, having optimized the antibacterial activity for three medically relevant Gram-negative bacteria, we proceeded to test the lead compound Api88 against a panel of seven clinically important pathogens (*i.e.*, 37 strains and clinical isolates) including nine drug-resistant strains (Table 2, also see Supplementary Table S1). Importantly, the MIC values were observed over a very narrow range (0.125−4 μg/mL), a promising result for the treatment of all clinically relevant Gram-negative pathogens currently causing concerns including *P. aeruginosa* and *A. baumannii*. As expected, Api88 was highly active against a single clinical isolate of *K. pneumoniae* KPC (*K. pneumoniae* carbapenemase; conferring resistance to all β-lactams except aztreonam) (MIC 2 μg/mL). A time-kill assay with *E. coli* BL21 AI performed at peptide concentrations corresponding to 10 × MIC showed that Api88 was bactericidal (*i.e.*, reducing the colony forming units (CFU) by more than

Table 2. Broad Spectrum Antimicrobial Activity of Lead Compound Api88 against Different Gram-Negative Pathogens[a]

pathogen	no. of strains and isolates tested	range of MIC values (μg/mL)
E. coli	8	0.5−1.0
K. pneumoniae	6	0.25−0.5
P. aeruginosa	8	1.0−4.0
A. baumannii	5	1.0−2.0
Enterobacter cloacae	5	0.25
Proteus vulgaris	5	0.125−1.0

[a]For details see Supplementary Table S1.

1000-fold within 24 h) and killed these bacteria quickly by reducing the CFU within the first 30 min by 10-fold, whereas the native sequence was less effective and only bacteriostatic (see Supplementary Figure S1). Even at a 10-fold lower concentration (*i.e.*, 1 × MIC), Api88 was still bactericidal and killed the bacteria relatively fast by reducing the bacterial load within the first 30 min by 90%.

Cellular Toxicity. Api88 did not influence the proliferation of SH-SY5Y-, HeLa-, HEK293-, and HepG2-cells (Figure 1).

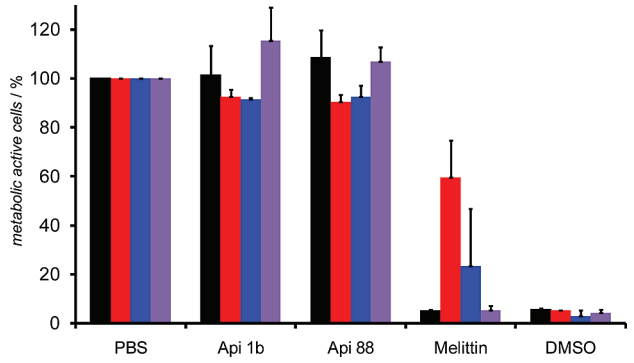

Figure 1. Cytotoxic effects of apidaecin 1b and its derivative Api88 against human embryonic kidney cells (HEK293; black bars), human hepatoma cells (HepG2; red bars), HeLa cells (blue bars), and differentiated SY5Y cells (purple bars). The cell lines were incubated with apidaecin 1b and Api88 at a concentration of 0.6 mg/mL for 24 h, *i.e.*, 285 and 262 μmol/L, respectively. The cell viability was determined with the Cell Proliferation Kit I. Positive controls consisted of DMSO (12%) and melittin (100 μg/mL, 35 μmol/L). The values were normalized to PBS (12%) as negative controls. The metabolic activity was determined twice in triplicates.

Moreover, it did not show any hemolytic effects on human red blood cells (see Supplementary Figure S2) within the tested concentration range up to 600 μg/mL, which is more than 100-fold above the MIC values.

Mode of Action. Although the detailed mechanism has not been determined for proline-rich AMP, all the evidence suggests that all members of this peptide family penetrate freely through the membrane of Gram-negative bacteria into the periplasmatic space, prior to dispersion within the cells. The latter step may involve an active transport process.[19] Once intracellular, it is assumed that the peptides block chaperone DnaK, as shown for pyrrhocoricin *in vitro* and also *in vivo* by bimolecular fluorescence complementation (BIFC).[20,21] This inhibition is lethal for *E. coli* at elevated temperatures, as indicated by DnaK null mutants of *E. coli* that do not survive at temperatures above 30 °C.[22] Therefore, the activity of proline-rich AMP depends on two factors, which most likely originate from different domains: the peptide uptake by the C-terminal sequence and inhibition of the intracellular target by the N-terminal sequence. As Api88 was developed stepwise from apidaecin 1b and resembled its structure closely, we assumed that the mode of action should be very similar, despite its higher net charge. Thus we compared Api88 with its native ancestor using a few key steps of the proposed mechanism. *In vitro*, a quartz crystal microbalance (QCM) was employed to compare the mass of Api88 taken up by a bacterial-mimetic membrane of composition DMPC:DMPG (4:1).[13,23−25] This method provided the mass of peptide binding by measurement of the frequency change of an oscillating crystal ($\Delta m \propto \Delta f$).[25,26] The mass of Api88 taken up into the lipid bilayer was found to increase over the concentration range 2−10 μmol/L (Figure 2, left), with membrane saturation occurring at ∼10 μM. Higher concentrations resulted in no further peptide binding (data not shown). The incorporation of Api88 was rapid and reversible in a manner similar to that observed for apidaecin 1b,[13] although the mass of peptide binding for Api88 (*cf.* apidaecin 1b) was greater at every concentration: 2 μmol/L (∼4.6 and ∼4.2 μg/mL), 7.3 (2) Hz; 5 μmol/L (∼11.5 and 10.5 μg/mL), 8.3 (2.5) Hz, and 10 μmol/L (∼23 and ∼21 μg/mL), 10.6 (3.5) Hz. These data support the uptake of peptide into bacterial (mimetic) membranes without disruption or irreversible change to the membrane layer. The reversibility of this peptide-membrane association is consistent with cell-penetrating peptides and facile intracellular transport.

A fluorescein labeled analogue of Api88 (CF-Api88) stained *E. coli*, *K. pneumoniae*, and *P. aeruginosa* within 60 min and was not removed from the cells by washing (see Supplementary Figure S3), whereas it was not able to enter HeLa cells within 2 h (data not shown). When the same experiment was repeated without washing Api88 (CF) off the cells, but in the presence of trypan blue to quench the fluorescence in the medium and at the bacterial surface, the bacterial cross section still showed a homogeneous fluorescence stain (Figure 2, right). This clearly indicates that Api88 enters the cells and does not permeabilize the membrane for trypan blue. In a fluorescence polarization assay, the same peptide was studied for its DnaK binding. The binding constants determined with recombinant full-length DnaK were 5.0 ± 1.2 μmol/L (∼11.5 ± 2.7 μg/mL) for Api88 and 6.3 ± 2.3 μmol/L (∼13.2 ± 4.8 μg/mL) for apidaecin 1b (see Supplementary Figure S4), indicating that the sequence optimization did not alter the binding to DnaK. Interestingly, the binding constants are very similar to other native and artificial Pro-rich AMP.[20,27] The N-terminal sequence corresponding to residues 1−8 of apidaecin 1b had only a slightly weaker binding constant of 17.3 ± 3.2 μmol/L, whereas the C-terminal part (residues 9−18) bound very weakly (33.1 ± 5.6 μmol/L) (see Supplementary Figure S4). This was further confirmed by a crystal structure of the substrate binding domain of DnaK (residues 389−607) in complex with an Api88 fragment (residues 3−11) that bound to DnaK as well as apidaecin 1b (K_D = 5.8 ± 1.7 μmol/L) (Figure 3, also see Supplementary Figure S5). Interestingly, Api88 (3−11) bound within the same crystal form in a forward as well as in a reverse direction to DnaK. In both binding modes residues 5−11 bound to DnaK. The reverse binding mode was unexpected insofar as the almost identical sequence of oncocin and pyrrhocoricin (Y^6LPRP^{10} compared to Y^7IPRP^{11} in Api88) binds only in the forward direction to DnaK.[27,28] However, the ability of DnaK to bind peptides in both directions has been

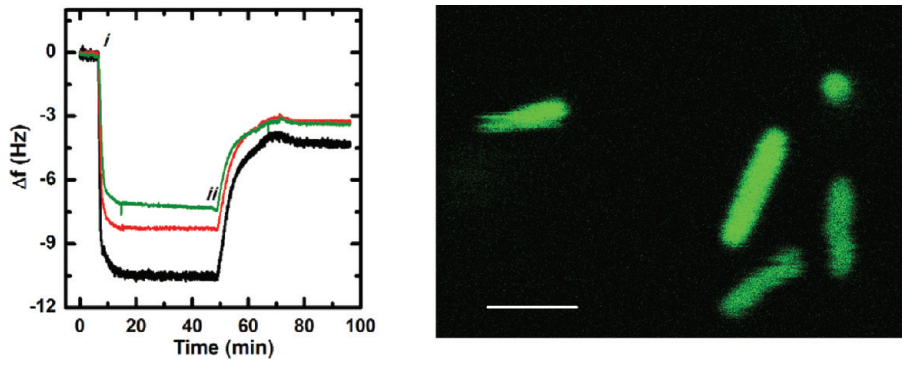

Figure 2. Quartz crystal microbalance (left) and confocal laser scanning microscopy image (right). The uptake of Api88 onto a preformed DMPC:DMPG (4:1) membrane layer is shown as a Δf–t graph; ***i*** indicates the beginning of the peptide and membrane interaction and ***ii*** corresponds to the introduction of the PBS buffer rinse in the QCM chamber. The Api88 concentrations were 2 μmol/L (green), 5 μmol/L (red), and 10 μmol/L (black) using the seventh harmonic. The fluorescence image was obtained by incubating an *E. coli* BL21 AI culture (3×10^8 cells/mL) with Api88(CF) (10 μmol/L) (60 min, 24 °C). The bar indicates 2.5 μm.

suggested previously following spectroscopic studies.[29] Both binding modes of the Api88 fragment appear to be stabilized by crystal packing interactions.

Substitution of glutamine in position 10 by arginine neither weakened nor strengthened the DnaK binding, which also agrees with the MIC values for *E. coli*. For *K. pneumoniae*, however, this substitution might strengthen the DnaK-binding and thereby the corresponding MIC values. Interestingly, apidaecin 1b and Api88 were highly active not only against *E. coli* MC4100 but also against two DnaK null mutants produced from this *E. coli* strain (see Supplementary Table S2). This clearly indicates that apidaecin 1b and the optimized Api88 do not only inhibit DnaK but can kill at least these *E. coli* strains equally efficient by inhibiting other intracellular targets, such as chaperonin GroEL and its cofactor GroES,[20,30] or even by a different mechanism. Such a second killing mechanism was suggested recently, based on the observation that cell division protease ftsH was overproduced in *E. coli* incubated with apidaecin 1b.[31] The authors speculated that the overexpressed protease will degrade cytoplasmic UDP-3-*O*-acyl-*N*-acetylglucoseamine deacetylase, resulting in an unbalanced synthesis of LPS and phospholipids. This multimodal killing mechanism should prevent or at least reduce the likelihood of possible resistance mechanisms caused by gene mutations or changes to the protein expression pattern.

All data suggest that Api88 kills Gram-negative bacteria by the same mechanism as apidaecin 1b, although its net charge at physiological conditions is around +7 compared to only +4 for apidaecin 1b due to substitutions in positions 2 (Orn) and 19 (Arg), a guanidated N-terminus, and an amidated C-terminus. To further confirm the suggested nonlytic target-inhibiting mechanism, the antimicrobial activity of Api88 was compared to its all-D and retro-inverso analogues. Whereas Api88 was highly active against two *E. coli* and two *K. pneumoniae* strains, the all-D and retro-inverso forms were at least 64-fold less active or even inactive (Table 3). This clearly indicates that the activity of Api88 depends on its stereospecific interaction with a transporter or target protein but not on lytic effects. It will be important for the further optimization of lead compound Api88 to study the underlying mechanisms in more detail.

Api88 Distribution in Mice. As all the available data suggested a broad antibiotic activity against the most threatening Gram-negative pathogens, without toxic side effects, we proceeded to test Api88 in mice. *In vivo* imaging showed that Api88 labeled at the side chain of the ornithine with DY675-Ser-Gly was systemically distributed within 30 min after intraperitoneal (i.p.) injection (see Supplementary Figure S6). These images were taken at different time points, and the fluorescence in the organs indicated that the peptide was effectively distributed throughout the body, although it is not possible to distinguish between the fluorescence of the full length peptide and any fluorescent degradation products. As the fluorescence-dye label coupled to the N-terminus of Api88 might influence the peptide distribution, we used an alternative approach that relied on Api88 labeled with ^{125}I at Tyr-7. This radioactive derivate was injected into the jugular vein of CD-1 mice, and its distribution was studied by measuring the radioactivity in six organs and in serum (Figure 4A). Interestingly, the radioactivity was detected at similar levels in liver and kidney, which confirms the unexpectedly high hepatic clearance of the polar, positively charged peptide as indicated by the *in vivo* imaging (see Supplementary Figure S6G). Importantly, fluorescence and radioactivity were detected in all organs studied and at high levels (only moderate in brain) clearly indicating that Api88 could target and kill bacteria in all parts of the body. As tissue distribution is not the most sensitive technique to characterize the permeability of the peptide toward the BBB,[32] this was studied by multiple time regression. The influx transfer constant (K_{in}) was 0.37 μL/(g × min) for Api88 with an apparent initial distribution volume (V_i) of 26.06 μL/g, compared to a K_{in} of 0.25 μL/(g × min)) and V_i of 14.27 μL/g for the almost impermeable marker bovine serum albumin (BSA) (Figure 4B). This represents a small but significant influx of Api88 from the serum into the brain, with a brain distribution volume almost double that of BSA. Given the specific activity of ^{125}I-Api88 (3.95 cpm/pg), about 0.7 ng reached the brain (0.5 g) within 10 min, which corresponds to a percentage ratio brain/serum of 3%. In order to distinguish the peptide distribution between brain parenchyma and blood-brain capillaries, a capillary depletion experiment was performed, demonstrating that a significant portion of the peptide had reached the brain parenchyma (77.5 ± 1.1%) rather than being trapped in the capillaries (22.5 ± 1.1%). Thus the amount of peptide entering the brain is mostly transferred from the capillaries to the parenchyma. The brain to blood transport (efflux) showed only a small efflux rate (k_{out} = 0.061 ± 0.075 min^{-1}), indicating that Api88 remains considerably longer in the brain tissue and is not rapidly transported back to

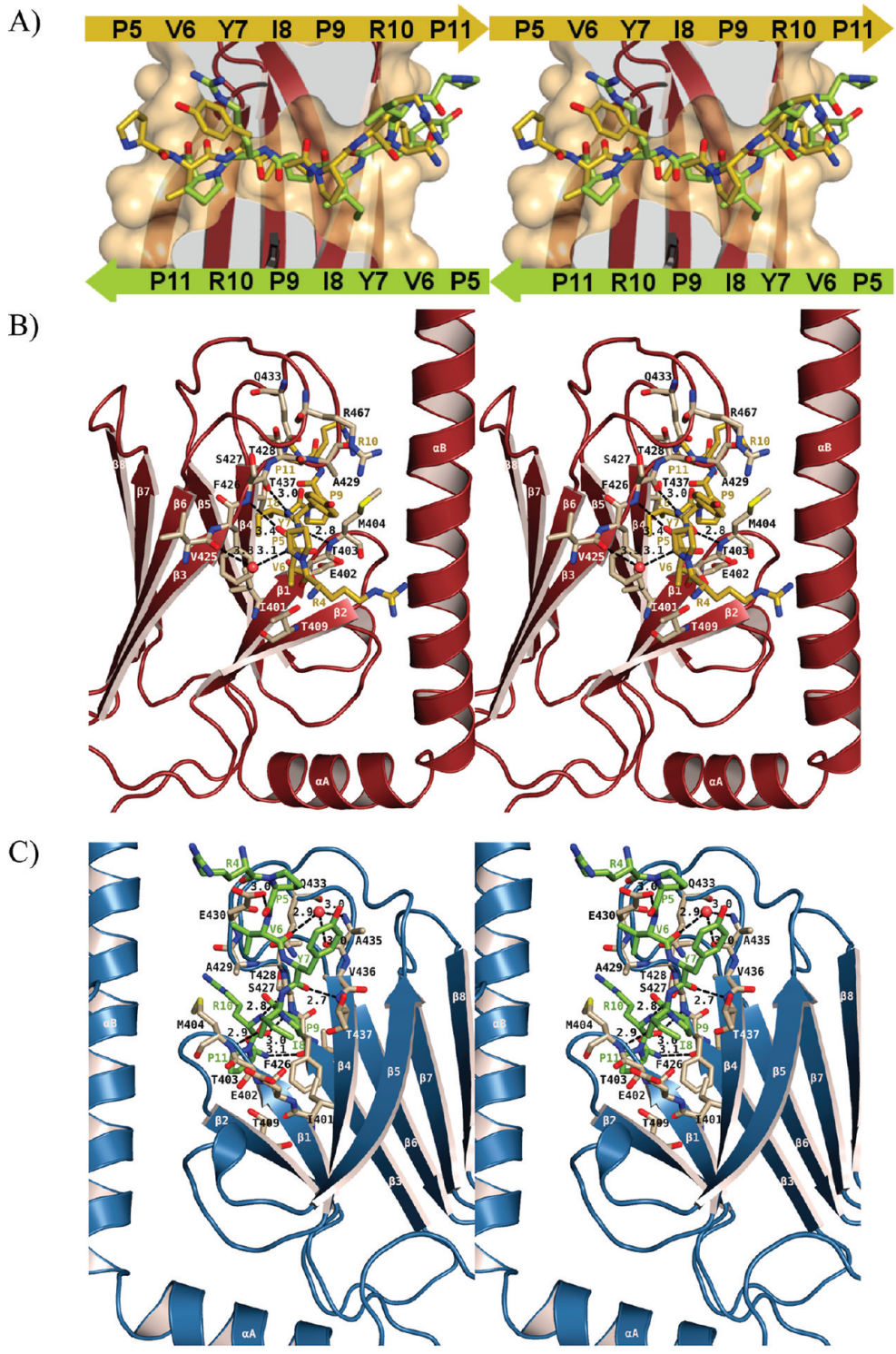

Figure 3. Stereoviews of the binding modes of an Api88 fragment (residues 3−11) to the substrate binding cleft of DnaK (residues 389−607). (A) This fragment binds in a forward (yellow carbon atoms) and in a reverse direction (green carbons) to the two independent DnaK molecules in the asymmetric unit of the crystal. The two binding modes are superimposed. In the forward and reverse binding modes, Ile-8 and Pro-9 occupy the central hydrophobic pockets, respectively. (B) Hydrogen bonding and van der Waals interactions between the forward binding Api88 fragment (yellow) and the substrate binding domain of DnaK (red). Residues 4−11 of the peptide are visible in the electron density. Two strong (≤3 Å) and two weak hydrogen bonds are formed. The peptide in the forward binding mode forms less strong hydrogen bonds to DnaK compared to the DnaK-oncocin interactions.[27] Superposition to the oncocin structure (Supplementary Figure S5) shows a shift of the peptide that may be caused by crystal contacts. This shift most likely results in the suboptimal interaction pattern of the peptide with DnaK, which is also reflected by relatively high B-factors of the peptide and partly weak electron density for a 1.9 Å structure, especially for residues 9−11 (not shown). (C) Stereoview of the hydrogen bonding and van der Waals interactions between the reverse binding Api88 fragment (green) and the substrate binding domain of DnaK (blue). Residues 4−11 of the peptide are visible in the electron density. Six strong (≤3 Å) and one weak hydrogen bonds are formed showing a tight

dx.doi.org/10.1021/cb300063v | *ACS Chem. Biol.* 2012, 7, 1281−1291

Figure 3. continued

interaction. The B-factors for the reverse binding peptide are lower as for the forward binding peptide and the electron density is well-defined (not shown).

Table 3. Sequence MIC Values Determined in 1% TSB of Api88, All-D-Api88, and Retro-inverso Api88 against Two *E. coli* and One *K. pneumoniae* Strains

		MIC (μg/mL)			
		E. coli		*K. pneumoniae*	
code	sequence[a]	ATCC 25922	DSM 10233	DSM 681	DSM 11678
Api88	Gu-ONNRPVYIPRPRPPHPRL-NH_2	2	1	2	8
All-D-Api88	Gu-onnrpvyiprprpphprl-NH_2	128	64	256	256
Retro-inverso-Api88	lrphpprprpiyvprnno-NH_2	>256	128	>256	>256

[a]Gu denotes *N,N,N′,N′*-tetramethylguanidine, O denotes L-ornithine, and small form letters denote D-amino acids.

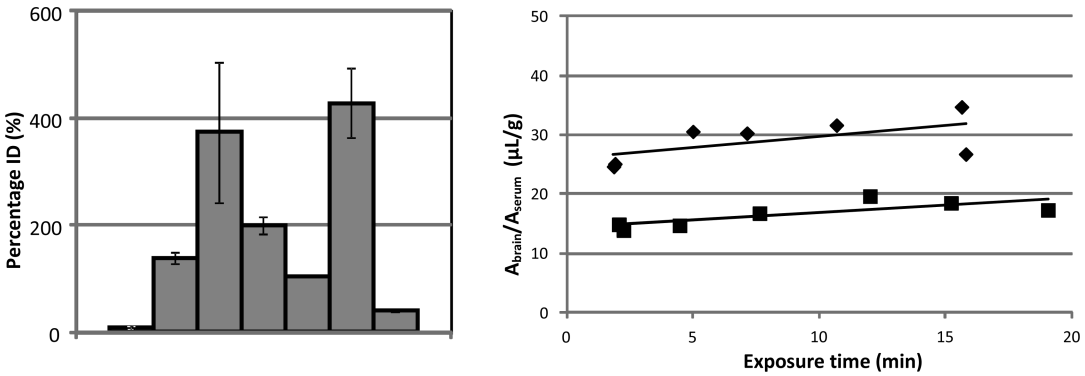

Figure 4. Distribution of ^{125}I-labeled Api88 in organs and serum after 15 min (left) and the brain influx of ^{125}I-labeled Api88 (right). The radiolabeled peptide (200 μL, 30,000 cpm/μL) was injected into the jugular vein of anesthetized CD-1 mice. At specified time points blood was obtained from the carotid artery, and the mouse was decapitated. Immediately after brain collection, spleen, liver, lungs, heart, and kidneys were collected and weighed. The percentage of time-corrected injected dose (ID) was then calculated from the measured gamma counts. Left: The bars represent the values calculated for brain, spleen, kidney, lungs, heart, liver, and serum (from left to right). Right: The brain influx multiple time regression of ^{125}I-Api88 (◆) *versus* ^{125}I-BSA (■) was calculated according to Gjedde.[46] The influx of ^{125}I-Api88 (*cf.* ^{125}I-BSA) was described by the linear regression $y = 0.37x + 26.06$ ($y = 0.25x + 14.27$).

the periphery. This global influx rate, however, is negatively influenced by the rapid and high hepatic and kidney clearance, reducing the serum concentration of Api88 passing through the brain, and hence a rapid declining exposure of Api88 to the brain tissue.

Toxicity in NMRI Mice. Seven healthy female NMRI outbred mice (~7 weeks old, 28−32 g) were treated with four doses of 20 mg/kg body weight (BW) of Api88 administered *via* i.p. bolus at 0, 3, 7, and 24 h. None of the animals showed any discomfort after the injections, and all mice showed their regular behavior and feeding pattern during the 5-day observation period. Following administration of a double dose, a few animals showed a slight discomfort after the first injection for up to 10 min, which was not observed after the three consecutive injections, but no other irregular behavior or feeding pattern. After 5 days the mice were sacrificed. The brain, kidney, pancreas, lung, urinary tract, genitals, and thymus all revealed a typical (normal) histology with no signs of inflammation, internal bleeding, or any other pathological finding (data not shown). Giemsa staining of the spleen sections did not reveal any additional basophil or eosinophil granulocyte infiltration (data not shown). The cellular architecture of the spleen was not altered in the Api88 treated mice (Figure 5C) compared with the PBS control (Figure 5D). Further histopathological investigation demonstrated no differences between the 20 and 40 mg/kg BW Api88 and the placebo groups for white pulp and red pulp of the spleen parenchyma (data not shown). Also, there were no differences in the histological appearance and the number of living cells per spleen (see Supplementary Figure S7) as well as the proportions of several splenocyte subpopulations, *i.e.*, neutrophilic granulocytes, macrophages, dendritic cells, natural killer cells, B cells, and T cells (Figure 5A). The expression of the activation marker CD86 on antigen-presenting cells was not influenced by Api88 (Figure 5B). The resulting data for peritoneal exudate cells were also similar to those of the splenocytes. There were no significant differences in the number of living peritoneal cells as well as the rate and activation levels of several peritoneal cell subpopulations (see Supplementary Figure S8). Taken together, no evidence was found for *in vivo* immunomodulatory activities of Api88, which contrasts a recent report about the *in vitro* effects of native apidaecin 1b.[33]

Murine Infection Models. The efficacy of Api88 was first evaluated in a systemic septicemia *E. coli* ATCC 25922 infection model (with 2.5% mucin) on female NMRI outbred mice (seven animals per group). Untreated mice (23−28 g) were extremely sick within 1 h and had to be euthanized based on a scoring system within 11 ± 3 h post infection. Bacteria were detected after 1 h in the blood and in the liver, lung,

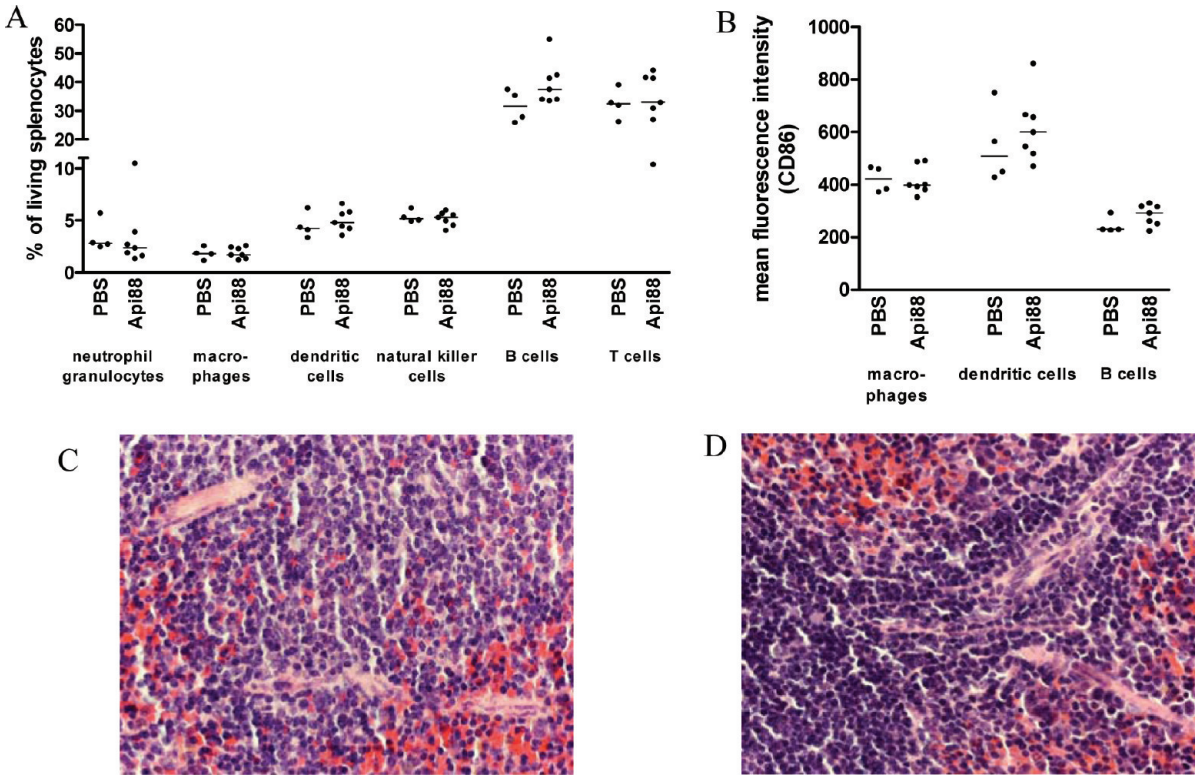

Figure 5. Influence of Api88 treatment on splenocyte subpopulations and their activation. Female NMRI outbred mice were treated with four doses of 20 mg/kg body weight (BW) Api88 (n = 7) or PBS (n = 4) as control. The rate of the splenocyte subpopulations (A) and the expression of the activation marker CD86 by professional antigen-presenting cells (B) were determined by flow cytometry analysis. The data shown are medians. Significance between the groups was determined by Mann−Whitney test. The immune cell subpopulations were identified by expression of specific markers, *i.e.*, neutrophilic granulocytes ($Gr1^{++}$, exclusion of eosinophilic granulocytes by counterstaining of SiglecF), macrophages ($CD11b^{+}$, $F4/80^{+}$, $CD11c^{-}$, $B220^{-}$), dendritic cells ($CD11c^{+}$), natural killer cells ($NKp46^{+}$, $CD3^{-}$), B cells ($B220^{+}$, $CD11c^{-}$, $CD11b^{-}$), and T cells ($CD3^{+}$, $B220^{-}$). The cellular architecture of the spleen of the PBS control (D) was not altered by the Api88 treatment (C) at a magnification of 400x (hematoxylin and eosin staining).

kidney, spleen, and brain with a further increase of the bacterial loads afterwards (see Supplementary Figure S9A). When treated with Api88 at i.p. bolus doses of 20, 10, 5, 2.5, or 1.25 mg/kg BW at three time points (1, 4, and 8 h post infection), the survival rates of the animals increased for all the doses to 100% (Figure 6A). The weight losses of the animals after infection increased with lower doses (see Supplementary Figure S9B). These weight changes correlated well with the scoring based on the clinical symptoms shown by the animals. The high-dose groups and the animals treated with ciprofloxacin recovered relatively fast, whereas the animals treated with the lowest dose needed ∼2 days to recover completely (see Supplementary Figure S9B). Similar to the toxicity study, the number of splenocytes or peritoneal exudate cells did not change in the infected animals that were treated with Api88 or ciprofloxacin (control) (see Supplementary Figure S10).

Finally, we tested Api88 in a second murine model (infection with *E. coli* Neumann as an clinical isolate; 1×10^7 CFU/mL) using female CFW-1 mice (5 animals per group, BW 20−25 g, 4−5 weeks) followed by treatment with Api88 (Figure 6B). The two highest doses provided a survival rate of 100%, whereas 80% and 40% of the animals survived after the lower doses of 5 and 2.5 mg/kg BW, respectively. When the peptide was administered in Kollidon FP17, a commercially available vehicle for injections in animals, the survival rate increased to 100% for animals treated at the same time intervals with a dose of 5 mg/kg. Interestingly, this reproducibly obtained ED_{100} was identical to the ED_{100} of imipenem, which was determined in the same infection model, later in the course of the experiments. However, the MIC values of imipenem and Api88 were 0.06 and 2 μg/mL, respectively, in 25% Mueller-Hinton broth for the clinical isolate *E. coli* Neumann. Considering that no adverse effects were observed with repeated i.p. injections of 40 mg/kg BW during the toxicity study and there was a 100% survival rate after administration of 5 mg/kg BW in both infection models, the MOS (margin of safety) was better than eight.

Although *E. coli* ATCC 25922 is commonly used for murine infection models,[34,35] and despite the fact that it was passaged twice through mice to increase its virulence, it is considered to be an only moderately pathogenic strain. Still the survival rates of the NMRI mice were very impressive, especially as the lower virulence was partially compensated by the relatively late therapeutic intervention (*i.e.*, 1 h post infection) allowing the bacteria to distribute systemically. In contrast, the *E. coli* Neumann strain is adapted for infection models and is rated to be suitable for an adequate sepsis model. It was used recently to evaluate A3-APO, a lead compound developed by combining sequences from different proline-rich AMP followed by chemical optimization.[16] At the lowest dose administered of 2.5 mg/kg BW Api88 four out of five CFW-1 mice survived significantly longer than the control group with only two of them surviving the 5 day observation period. When Api88 was

dx.doi.org/10.1021/cb300063v | *ACS Chem. Biol.* 2012, 7, 1281−1291

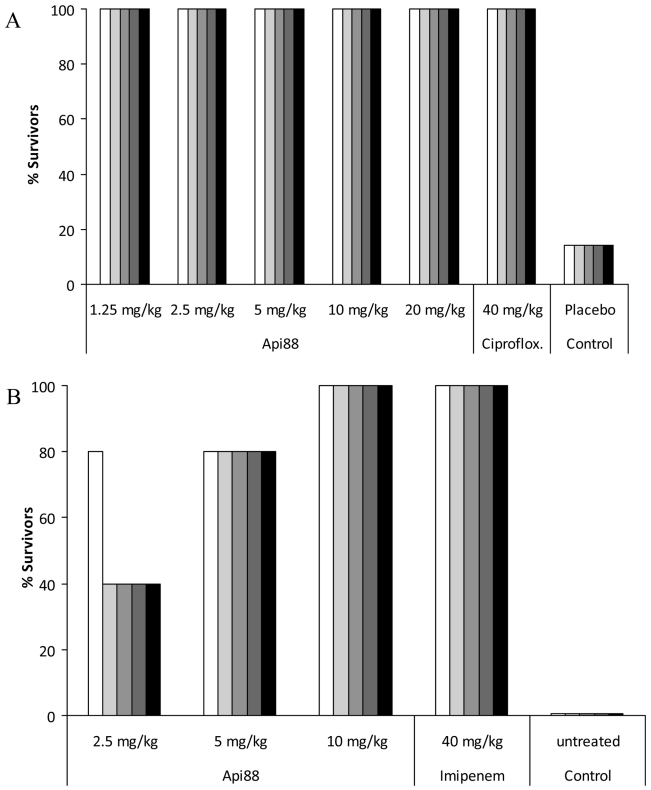

Figure 6. Survival rates of NMRI (A, seven per group) and CFW1 (B, five per group) mice after infecting them with *E. coli* ATCC 25922 and *E. coli* Neumann, respectively. NMRI mice were treated 1, 4, and 8 h post infection using an individual dose of 20, 10, 5, 2.5, or 1.25 mg/kg BW Api88. Ciprofloxacin was injected at a dose of 40 mg/kg BW as positive control. CFW1 mice were treated 0.5, 4, and 8 h post infection with individual doses of 10, 5, or 2.5 mg/kg BW Api88 or 40 mg/kg imipenem as control (vehicle only). Shown are the survival rates of all animal groups 12 h (white bar) and 2 (light gray), 3 (gray), 4 (dark gray), and 5 days (black) post infection.

administered i.p. in a polyvinylpyrrolidone (PVP) formulation, the ED_{100} was 5 mg/kg BW. Thus, Api88 and imipenem were equally effective in the *E. coli* Neumann infection model, whereas imipenem was 30-fold more active *in vitro* based on the MIC values. This is in line with observations from Otvos for A3-APO.[16] Similar apparent contradictions were also reported for other AMP and indicated that the MIC values of peptides cannot always be simply extrapolated to murine models using the expert knowledge obtained for small molecules.

In addition, the peptide brain distribution showed a brain-serum ratio of 3% indicating that the peptide significantly entered the brain parenchyma, rather than being trapped in the blood-brain capillaries. Once in the brain, Api88 remained there for a long time, apparent from the small efflux and low metabolism rate. Considering a therapeutic dose of 10 mg/kg BW Api88 (*i.e.*, 250 μg Api88 per mouse) and a total blood volume of 2.5 mL per mouse, the maximal Api88 concentration in blood should be around 100 μg/mL and about 3 μg/mL in CSF. This is still above the MIC value determined for *E. coli* Neumann in 25% MHB medium. As the activity of apidaecin 1b and most other cationic AMP increases with lower salt concentrations as found in the CSF, Api88 appears to be a suitable treatment option for infections of the CNS.

One explanation for the high *in vivo* activity might be additional immunomodulatory effects of AMP that are not considered in antibacterial *in vitro* assays but may be significant toward animals. Thus AMP could act by two independent mechanisms *in vivo*. First, they could kill the pathogens directly, when injected at high doses somewhat similar to the *in vitro* testing. In parallel, the immune system might be stimulated and initiate the fight with pathogens even after the peptides were cleared from the body or degraded by proteases. Such immunomodulatory effects are well-known for mammalian HDP with *in vitro* antimicrobial activities, such as defensins or cathelicidins.[36−41] More surprising was a recent finding that apidaecin 1b has immunomodulatory effects on human macrophages and monocytes *in vitro* despite the evolutionary distance between honey bees and humans.[33] We did not find any evidence for immunomodulatory side effects here for Api88 with NMRI mice, such as modulation of the activation state of antigen-presenting cells from spleen or the peritoneal cavity or proliferative effects on splenocytes or peritoneal exudate cells. At this point it remains unclear if this effect is related to the modified sequence of Api88, differences between the murine and human immune systems or if the effect was just too weak to be identified in the mouse model at the studied time points. All of these questions need to be addressed in future studies.

In conclusion, the Api88 peptide is a highly efficient treatment for Gram-negative pathogens systemically with a therapeutic window larger than ten. Importantly, Api88 killed *E. coli* in a direct manner without apparent modulation of the immune system. This latter aspect will make it easier to develop Api88 further for clinical applications, as its mode of action can be directly linked to specific inhibition of the substrate binding domain of DnaK without any toxic effects toward human cells. Most importantly, Api88 was not able to enter HeLa cells, which provides an additional layer of safety. Future animal studies will be used as added proof that the low MIC values obtained for *K. pneumoniae*, *P. aeruginosa*, and *A. baumannii* allow also treating such systemic infections.

METHODS

Peptide Synthesis. Peptides were synthesized as C-terminal amides or free acids with standard 9-fluorenylmethoxycarbonyl/*tert*-butyl (Fmoc/*t*Bu) chemistry at the 25 or 250 μmol scale using diisopropyl carbodiimide (DIC) or 2-(1*H*-benzotriazol-1-yl)-1,1,3,3-tetramethyluronoium hexafluorphosphate (HBTU) activation (for details see Supporting Information).[42] HBTU activation was also used to manually couple acetic acid ("acetylation") or 5,(6)-carboxyfluoresceine to the unprotected N-termini after completion of the peptide synthesis. The *N*,*N*,*N*′,*N*′-tetramethylguanidino group was obtained by incubating the N-terminally deprotected peptides with 10 equiv of HBTU and *N*-methymorpholine.[43] For *in vivo* imaging, Api88 was synthesized with methyltritryl-protected ornithine, which was selectively deprotected after N-terminal guanidation. The peptide synthesis was continued at the δ-amino group of ornithine by coupling glycine and serine before the fluorescence dye DY675 (0.5 equiv, Dyomics GmbH, Jena, Germany) was coupled to the α-amino group of serine. All peptides were cleaved with trifluoroacetic acid (TFA), precipitated with cold diethyl ether and finally purified on a C_{18}-phase using a linear aqueous acetonitrile gradient in the presence of 0.1% (v/v) TFA as ion pair reagent. The purified peptide was analyzed by analytical RP-HPLC and matrix-assisted laser desorption/ionization time-of-flight mass spectrometry. For the animal studies, the lyophilized peptides were dissolved in 0.1% (v/v) aqueous acetic acid and lyophilized twice to remove residual TFA. The tissue distribution and multiple time regression studies relied on purified Api88 and BSA (control), which were labeled with ^{125}I by the Iodogen method and purified over Ag filters (for details see Supporting Information). The

^{125}I-Api88 purity was assessed by RP-HPLC, which confirmed also that the filtrate did not contain any free iodide.

Antibacterial Activity.[27] MIC values for *E. coli* (strains BL21 AI, D31, MC4100, ATCC 25922, DSM 10233, ΔDnaK, and ΔDnaK52) and *K. pneumoniae* (K6, DSM 681, and DSM 11678) were determined in triplicate by a liquid broth microdilution assay in sterile 96-well plates using a 2-fold peptide dilution series in 1% (w/v) tryptic soy broth (TSB; 33% TSB medium) (for details see Supporting Information). The inoculum (50 μL, 1.5 × 10^7 cells/mL) was prepared by diluting an overnight culture grown in nutrient broth (Carl Roth GmbH, Karlsruhe, Germany) with 33% TSB medium. The MIC values of all other pathogenic bacteria were tested in 1% TSB medium using an overnight culture grown on Columbia agar (Becton Dickinson, Sparks, MD, USA) at 37 °C and diluted with 1% TSB medium first to an $OD_{578\ nm}$ of 0.1 and then further 285-fold (inoculum: 190 μL, (1−2) × 10^5 CFU/mL). All plates were incubated at 37 °C for 18 h, except the null mutants ΔDnaK and ΔDnaK52 (courtesy of B. Bukau, MPI, Heidelberg) that were grown at 30 °C. The MIC was defined as the lowest peptide concentration preventing visible bacterial growth.

DnaK Expression, Crystallization, and Structure Determination. The substrate binding domain (SBD) of *E. coli* DnaK (residues 389−607) and the full length protein were expressed and purified as described.[44] The SBD was concentrated to 16 g/L, mixed with Api88 (residues 3−11) at a 1:5 molar ratio and incubated (1 h, RT).[28] Crystals were grown with the hanging-drop vapor diffusion method in 2.7 mol/L ammonium sulfate and 0.1 mol/L MES (pH 6.0). These crystals could be cooled to 100 K for data collection without the need to add a cryo protectant. Diffraction data were collected at the Bessy synchrotron beamline 14.1 to a resolution of 1.9 Å and processed using XDS[45] and SCALA[46] (Supplementary Table S1). The structure was solved by molecular replacement using Molrep[47] and PDB ID 1DKZ.[44] The model was built with Coot[48] and refined with REFMAC.[49] The asymmetric unit contains two protein monomers (chain A and B) and two apidaecin peptides (chain C and D).

Fluorescence Polarization. The binding constants were determined with full length DnaK and 5(6)-carboxyfluorescein labeled peptides in polarization buffer (20 mmol/L TRIS, 0.15 mol/L KCl, 5 mmol/L $MgCl_2$, 1 mmol/L NaN_3, and 2 mmol/L dithiothreitol, pH 7.5) at 28 °C, as described recently.[27] Briefly, black 384-well plates (flat bottom, Greiner Bio-One GmbH) were blocked with 0.5% (w/v) casein in washing buffer (10 mmol/L sodium phosphate, 0.3 mol/L NaCl, pH 7.4, and 0.05% (v/v) Tween20) at RT for 1 h and washed three times with washing buffer. A 2-fold dilution series of full length DnaK (40 μL/well) in polarization buffer containing a labeled peptide (10 nmol/L) was added and incubated (28 ± 1 °C). After 2 h the fluorescence anisotropy was measured on a Paradigm microplate reader (Beckman Coulter, Salzburg, Austria) in top read position (λ_{exc} = 485 nm, λ_{em} = 535 nm) on at least two different days in triplicates. The data were fitted to a nonlinear, dose−response logistical transition $[y = a_0 + a_1/(1 + x/a_2)^{a_3}]$ using the Levenberg−Marquardt algorithm with the dissociation constants (K_D) being represented by the a_2 coefficients (SlideWrite, Encinitas, CA, USA.).

Cytotoxicity. Cell viabilities were determined with the MTT cell proliferation assay[50,51] for human embryonic kidney (HEK 293), human hepatoma (HepG2-), SH-SY5Y-, and HeLa-cells (for details see Supporting Information). The cell lines were cultured in DMEM/Ham's F-12 medium containing fetal bovine serum, neomycin, penicillin, and streptomycin, seeded (2 × 10^4 cells) in the same medium into 96-well plates and incubated (overnight, 37 °C, 5% CO_2) or differentiated with *trans*-retinoic acid (SY5Y, 10 μmol/L, 5 days). Peptide solutions (0.6 g/L) were added to the cells washed with phosphate buffered saline (PBS) and incubated again at identical conditions for 24 h.

Hemolytic Activity.[18] Concentrated human erythrocytes were washed, suspended in PBS (2%, 50 μL), and added to a serial peptide dilution series from 600 to 5 μg/mL in PBS (50 μL) in 96-well polypropylene plates (V-bottom, Greiner Bio-One GmbH) and incubated (37 °C, 1 h). After centrifugation (1000*g*) the absorbance of the supernatants was determined in a 384-well plate (flat-bottom, Greiner Bio-One GmbH) at 405 nm in a Paradigm microplate reader. The positive and negative controls were 0.1% triton X-100, melittin (75 to 0.6 μg/mL) and PBS, respectively.

Fluorescence Microscopy. *E. coli* ATCC 25922, *K. pneumoniae* DSM 681, and *P. aeruginosa* DSM 3227 were grown overnight in nutrient broth and diluted with 33% TSB medium. Api88 labeled N-terminally with 5(6)-carboxyfluorescein was added to the cell suspension (8 × 10^7 cells/mL) at a final concentration of 125 μg/mL, incubated (90 min, 37 °C), and centrifuged (12000*g*). The cells were washed twice with sterile NaCl solution (0.9%) and once with water (600 μL each) and resuspended in water (50 μL). One-fifth of the suspension was dried on a microscope dish (darkness), embedded (mowiol mounting solution), and covered with a coverslip, and the fluorescence was measured on a confocal laser scanning microscope TCS SP5 (Leica Microsystems, Wetzlar, Germany).

Alternatively, *E. coli* BL21 AI (3 × 10^8 cells/mL) were incubated with Api88 labeled at the side chain of Orn-1 with 5(6)-carboxyfluorescein (10 μmol/L, ∼1.5-fold MIC) at RT (60 min). The background fluorescence was quenched with trypan blue (10 μL, 1 g/L),[52] and the fluorescence was measured on the confocal laser scanning microscope TCS SP5.

Animal Studies. All experiments started after an acclimatization period of at least 3 days in accordance with FELASA and GV-Solas guidelines. The animal studies were approved by the Animal Care and Usage Committee of the state agency (Landesdirektion Leipzig, file number: 24-9168.11/12/22).

Api88 Distribution in Mice. Female NMRI outbred mice (40−45 g, 12 weeks) were anesthetized with ketamine (100 mg/kg BW) and medetomidine (1 mg/kg BW) in sterile NaCl solution (0.9%, 200 μL i.p.). DY675-Api88 (40 μg in 200 μL sterile PBS) was injected i.p., and the fluorescence was measured on a NightOWL II LB 983 (Berthold Technologies GmbH, Bad Wildbad, Germany) with the following parameters: λ_{ex} = 630 ± 20 nm, λ_{em} = 720 ± 20 nm, sample size 129.873, sample height 55, camera gain low, camera readout fast, exposure time 1.0 or 0.1 s (Photo), and illumination 0 or 10 (Photo). The mice were euthanized with CO_2, and the organs were analyzed using the same parameters.

Male Caesarean Derived-1 mice from the Institute for Cancer Research (ICR-CD-1, Harlan Laboratories, Venray, The Netherlands; 25−30 g) were used according to the Ethical Committee principles of laboratory animal welfare as approved by our institute (Ghent University, Faculty of Veterinary Medicine, 2009-052). CD-1 mice were anesthetized with urethane (i.p., 3 g/kg BW), and the jugular vein and carotid artery were isolated. ^{125}I-Api88 (30 000 cpm/μL) and ^{125}I-BSA were injected separately into the jugular vein. The radioactivity was determined after specified time periods in serum (prepared from blood collected from the carotid artery) and different organs (brain, spleen, kidney, liver, lung, heart) after decapitation (for details see Supporting Information). The theoretical background of the multiple time regression analysis is based on the Gjedde equation.[53] The experiments were performed in duplicate.

Capillary depletion, *i.e.*, the extent of ^{125}I-Api88 crossing the capillary wall into the brain parenchyma instead of being trapped in the capillary cells, was determined by the method of Triguero *et al.*[54] as modified by Gutierrez *et al.*[55] (for details see Supplementary). Briefly, the peptide was injected into the jugular vein of anesthetized CD-1 mice. Blood was collected from the abdominal aorta and the brain was perfused manually, before it was collected, homogenized, weighed, and separated by centrifugation into the capillaries (pellet) and parenchyma and fat tissues (supernatant). Compartmental BBB distribution was evaluated from plotting capillaries/serum and parenchyma/serum activity ratios *versus* time (n = 2).

NMRI Mouse Model. Acute toxicity of Api88 was studied for doses of 20 and 40 mg/kg BW by injecting either dose four times (0, 3, 7, and 24 h) into NMRI mice (28−32 g, ∼7 weeks old). The antibacterial therapy was done with NMRI mice (25−28 g, 6−8 weeks old) infected with a lethal dose of *E. coli* strain ATCC 25922 (1.1 ± 0.2 × 10^6 CFU in the presence of 2.5% (w/v) mucin, i.p.).[56] Api88 (20 to 1.25 mg/kg BW) and ciprofloxacin (40 mg/kg BW) were dissolved

in aqueous glucose solution (5% w/v) and administered three times i.p. (1, 4, and 8 h post infection). As negative control the glucose solution was added at the same time intervals. Mice were checked 3 times per day for the health status (mobility, breathing, feeding, fur appearance (plain or scrubby), *etc.*) for a total period of 5 days and weighed 1 day before and 1 and 5 days after infection, before the organs were removed and analyzed histopathologically. Moribund mice were euthanized in accordance with the Animal Care and Usage Committee of the Landesdirektion Leipzig.

For splenocyte analyses residual spleen not needed for the histopathological analysis was used for preparation of a single cell suspension. The portions of splenocyte subpopulations and the expression of the activation marker CD86 by professional antigen-presenting cells were determined by flow cytometry analysis. The different immune cell subpopulations were identified by their expression of the following markers: neutrophilic granulocytes ($Gr1^{++}$, exclusion of eosinophilic granulocytes by counterstaining of SiglecF), macrophages ($CD11b^{+}$, $F4/80^{+}$, $CD11c^{-}$, $B220^{-}$), dendritic cells ($CD11c^{+}$), B cells ($B220^{+}$, $CD11c^{-}$, $CD11b^{-}$), and T cells ($CD3^{+}$, $B220^{-}$).

CFW-1 Mouse Infection Model. Female CFW-1 mice (body weight 20−25 g; 4−5 weeks of age) were infected i.p. with *E. coli* Neumann (an *E. coli* strain, adapted for mouse infection models) with an inoculum of $\sim 10^{7}$ CFU/mL in a final volume of 200 μL in 0.9% aqueous NaCl per animal. Peptides were dissolved in aqueous PVP (Kollidon FP17) and administered i.p. covering a dose range of 0, 2.5, 5, 10, 20 mg/kg at 0.5, 4, and 8 h post infection. Imipenem (injected as imipenem/cilastatin (500 mg/500 mg); trade name Zienam, Msd Sharp & Dohme GmbH, Haar, Germany) was administered in a dose range of 5, 10, 40 mg/kg with the same schedule. Survival of the mice was monitored every 4 h (except night time) during the first day of treatment and daily inspections afterward until day 5 post treatment.

■ ASSOCIATED CONTENT

Supporting Information

This material is available free of charge *via* the Internet at http://pubs.acs.org.

■ AUTHOR INFORMATION

Corresponding Author

*E-mail: Hoffmann@chemie.uni-leipzig.de.

Notes

The authors declare the following competing financial interest(s): R.H. is a cofounder of AMP-Therapeutics GmbH (Leipzig, Germany) and was appointed to their scientific advisory board in 2010.

■ ACKNOWLEDGMENTS

G.A., R.H., and N.S. were supported by the European Fund for Regional Structure Development (EFRE, European Union and Free State Saxony) by grants 13408/2286 (G.A.), 13405/2286 and 4-0123.55-20-0631-05/4 (both to R.H.), and 13406/2286 (N.S.) and the "Bundesministerium für Bildung und Forschung" BMBF by Innoprofile (R.H.). S.V.D. and B.D.S. were supported by the Institute for the Promotion of Innovation through Science and Technology in Flanders (IWT No. 73402).

We thank Manuela Fritsch, Agneta Mewes, Sarah Leitenroth, and Monique Richter for technical assistance during the animal studies; Prof. Dr. Peter Seibel and Dr. Ingo Schäfer for recording the confocal microscope images; and the Joint Berlin MX Laboratory at the Helmholtz Zentrum Berlin (Bessy II) for beam time and assistance during synchrotron data collection, as well as for traveling support.

■ REFERENCES

(1) Kotra, L. P., Golemi, D., Vakulenko, S., and Mobashery, S. (2000) Bacteria fight back. *Chem. Ind.*, 341−344.

(2) D'Costa, V. M., King, C. E., Kalan, L., Morar, M., Sung, W. W. L., Schwarz, C., Froese, D., Zazula, G., Calmels, F., Debruyne, R., Golding, G. B., Poinar, H. N., and Wright, G. D. (2011) Antibiotic resistance is ancient. *Nature 477*, 457−461.

(3) Michalopoulos, A., and Falagas, M. E. (2010) Treatment of Acinetobacter infections. *Expert Opin. Pharmacother. 11*, 779−788.

(4) Kumarasamy, K. K., Toleman, M. A., Walsh, T. R., Bagaria, J., Butt, F., Balakrishnan, R., Chaudhary, U., Doumith, M., Giske, C. G., Irfan, S., Krishnan, P., Kumar, A. V., Maharjan, S., Mushtaq, S., Noorie, T., Paterson, D. L., Pearson, A., Perry, C., Pike, R., Rao, B., Ray, U., Sarma, J. B., Sharma, M., Sheridan, E., Thirunarayan, M. A., Turton, J., Upadhyay, S., Warner, M., Welfare, W., Livermore, D. M., and Woodford, N. (2010) Emergence of a new antibiotic resistance mechanism in India, Pakistan, and the UK: a molecular, biological, and epidemiological study. *Lancet Infect. Dis. 10*, 597−602.

(5) Kumarasamy, K., and Kalyanasundaram, A. (2012) Emergence of Klebsiella pneumoniae isolate co-producing NDM-1 with KPC-2 from India. *J. Antimicrob. Chemother. 67*, 243−244.

(6) Khan, N. A. (2008) Acanthamoeba and the blood-brain barrier: the breakthrough. *J. Med. Microbiol. 57*, 1051−1057.

(7) Mariani, M. M., and Kielian, T. (2009) Microglia in infectious diseases of the central nervous system. *J. Neuroimmune Pharmacol. 4*, 448−461.

(8) Rock, R. B., Gekker, G., Hu, S. X., Sheng, W. S., Cheeran, M., Lokensgard, J. R., and Peterson, P. K. (2004) Role of microglia in central nervous system infections. *Clin. Microbiol. Rev. 17*, 942−964.

(9) Brogden, K. A. (2005) Antimicrobial peptides: Pore formers or metabolic inhibitors in bacteria? *Nat. Rev. Microbiol. 3*, 238−250.

(10) Otvos, L. (2002) The short proline-rich antibacterial peptide family. *Cell. Mol. Life Sci. 59*, 1138−1150.

(11) Casteels, P., Ampe, C., Jacobs, F., Vaeck, M., and Tempst, P. (1989) Apidaecins - Antibacterial peptides from honeybees. *EMBO J. 8*, 2387−2391.

(12) Casteels, P., and Tempst, P. (1994) Apidaecin-type peptide antibiotics function through a non-poreforming mechanism involving stereospecificity. *Biochem. Biophys. Res. Commun. 199*, 339−345.

(13) Piantavigna, S., Czihal, P., Mechler, A., Richter, M., Hoffmann, R., and Martin, L. L. (2009) Cell penetrating apidaecin peptide interactions with biomimetic phospholipid membranes. *Int. J. Pept. Res. Ther. 15*, 139−146.

(14) Casteels, P., Romagnolo, J., Castle, M., Casteelsjosson, K., Erdjumentbromage, H., and Tempst, P. (1994) Biodiversity of apidaecin-type peptide antibiotics - prospects of manipulating the antibacterial spectrum and combating acquired-resistance. *J. Biol. Chem. 269*, 26107−26115.

(15) Ostorhazi, E., Holub, M. C., Rozgonyi, F., Harmos, F., Cassone, M., Wade, J. D., and Otvos, L., Jr. (2011) Broad-spectrum antimicrobial efficacy of peptide A3-APO in mouse models of multidrug-resistant wound and lung infections cannot be explained by in vitro activity against the pathogens involved. *Int. J. Antimicrob. Agents 37*, 480−484.

(16) Szabo, D., Ostorhazi, E., Binas, A., Rozgonyi, F., Kocsis, B., Cassone, M., Wade, J. D., Nolte, O., and Otvos, L. (2010) The designer proline-rich antibacterial peptide A3-APO is effective against systemic Escherichia coli infections in different mouse models. *Int. J. Antimicrob. Agents 35*, 357−361.

(17) Benincasa, M., Pelillo, C., Zorzet, S., Garrovo, C., Biffi, S., Gennaro, R., and Scocchi, M. (2010) The proline-rich peptide Bac7(1−35) reduces mortality from Salmonella typhimurium in a mouse model of infection. *BMC Microbiol. 10*, 178.

(18) Knappe, D., Kabankov, N., and Hoffmann, R. (2011) Bactericidal oncocin derivatives with superior serum stabilities. *Int. J. Antimicrob. Agents 37*, 166−170.

(19) Scocchi, M., Tossi, A., and Gennaro, R. (2011) Proline-rich antimicrobial peptides: converging to a non-lytic mechanism of action. *Cell. Mol. Life Sci. 68*, 2317−2330.

(20) Otvos, L., O, I., Rogers, M. E., Consolvo, P. J., Condie, B. A., Lovas, S., Bulet, P., and Blaszczyk-Thurin, M. (2000) Interaction between heat shock proteins and antimicrobial peptides. *Biochemistry 39*, 14150−14159.
(21) Morell, M., Czihal, P., Hoffmann, R., Otvos, L., Aviles, F. X., and Ventura, S. (2008) Monitoring the interference of protein-protein interactions in vivo by bimolecular fluorescence complementation: the DnaK case. *Proteomics 8*, 3433−3442.
(22) Bukau, B., and Walker, G. C. (1989) Delta-Dnak52 mutants of Escherichia coli have defects in chromosome segregation and plasmid maintenance at normal growth temperatures. *J. Bacteriol. 171*, 6030−6038.
(23) Knappe, D., Piantavigna, S., Hansen, A., Mechler, A., Binas, A., Nolte, O., Martin, L. L., and Hoffmann, R. (2010) Oncocin (VDKPPYLPRPRPPRRIYNR-NH2): A novel antibacterial peptide optimized against Gram-negative human pathogens. *J. Med. Chem. 53*, 5240−5247.
(24) Mechler, A., Praporski, S., Atmuri, K., Boland, M., Separovic, F., and Martin, L. L. (2007) Specific and selective peptide-membrane interactions revealed using quartz crystal microbalance. *Biophys. J. 93*, 3907−3916.
(25) McCubbin, G. A., Praporski, S., Piantavigna, S., Knappe, D., Hoffmann, R., Bowie, J. H., Separovic, F., and Martin, L. L. (2011) QCM-D fingerprinting of membrane-active peptides. *Eur. Biophys. J. Biophys. Lett. 40*, 437−446.
(26) Sauerbrey, G. (1959) Verwendung Von Schwingquarzen Zur Wagung Dunner Schichten und Zur Mikrowagung. *Z. Phys. 155*, 206−222.
(27) Knappe, D., Zahn, M., Sauer, U., Schiffer, G., Strater, N., and Hoffmann, R. (2011) Rational design of oncocin derivatives with superior protease stabilities and antibacterial activities based on the high-resolution structure of the oncocin-DnaK complex. *ChemBioChem 12*, 874−876.
(28) Liebscher, M., and Roujeinikova, A. (2009) Allosteric coupling between the lid and interdomain linker in DnaK revealed by inhibitor binding studies. *J. Bacteriol. 191*, 1456−1462.
(29) Tapley, T. L., Cupp-Vickery, J. R., and Vickery, L. E. (2005) Sequence-dependent peptide binding orientation by the molecular chaperone DnaK. *Biochemistry 44*, 12307−12315.
(30) Zhou, Y. S., and Chen, W. N. (2011) iTRAQ-coupled 2-D LC-MS/MS analysis of cytoplasmic protein profile in Escherichia coli incubated with apidaecin IB. *J. Proteomics 75*, 511−516.
(31) Zhou, Y. S., and Chen, W. N. (2011) iTRAQ-coupled 2-D LC-MS/MS analysis of membrane protein profile in Escherichia coli incubated with apidaecin IB. *Plos ONE 6*, e20442.
(32) Van Dorpe, S., Bronselaer, A., Nielandt, J., Stalmans, S., Wynendaele, E., Audenaert, K., Van De Wiele, C., Burvenich, C., Peremans, K., Hsuchou, H., De Tre, G., and De Spiegeleer, B. (2011) Brainpeps: the blood-brain barrier peptide database. *Brain Struct. Funct.*, DOI: 10.1007/s00429-011-0375-0.
(33) Tavano, R., Segat, D., Gobbo, M., and Papini, E. (2011) The honeybee antimicrobial peptide apidaecin differentially immunomodulates human macrophages, monocytes and dendritic cells. *J. Innate Immun. 3*, 614−622.
(34) van Ogtrop, M. L., Andes, D., Stamstad, T. J., Conklin, B., Weiss, W. J., Craig, W. A., and Vesga, O. (2000) In vivo pharmacodynamic activities of two glycylcyclines (GAR-936 and WAY 152,288) against various gram-positive and gram-negative bacteria. *Antimicrob. Agents Chemother. 44*, 943−949.
(35) Andes, D., and Craig, W. A. (2006) Pharmacodynamics of a new cephalosporin, PPI-0903 (TAK-599), active against methicillin-resistant Staphylococcus aureus in murine thigh and lung infection models: Identification of an in vivo pharmacokinetic-pharmacodynamic target. *Antimicrob. Agents Chemother. 50*, 1376−1383.
(36) Biragyn, A., Surenhu, M., Yang, D., Ruffini, P. A., Haines, B. A., Klyushnenkova, E., Oppenheim, J. J., and Kwak, L. W. (2001) Mediators of innate immunity that target immature, but not mature, dendritic cells induce antitumor immunity when genetically fused with nonimmunogenic tumor antigens. *J. Immunol. 167*, 6644−6653.
(37) Biragyn, A., Ruffini, P. A., Leifer, C. A., Klyushnenkova, E., Shakhov, A., Chertov, O., Shirakawa, A. K., Farber, J. M., Segal, D. M., Oppenheim, J. J., and Kwak, L. W. (2002) Toll-like receptor 4-dependent activation of dendritic cells by beta-defensin 2. *Science 298*, 1025−1029.
(38) Biragyn, A., Coscia, M., Nagashima, K., Sanford, M., Young, H. A., and Olkhanud, P. (2008) Murine beta-defensin 2 promotes TLR-4/MyD88-mediated and NF-kappa B-dependent atypical death of APCs via activation of TNFR2. *J. Leukocyte Biol. 83*, 998−1008.
(39) Funderburg, N., Lederman, M. M., Feng, Z., Drage, M. G., Jacllowsky, J., Harding, C. V., Weinberg, A., and Sieg, S. F. (2007) Human beta-defensin-3 activates professional antigen-presenting cells via Toll-like receptors 1 and 2. *Proc. Natl. Acad. Sci. U.S.A. 104*, 18631−18635.
(40) Kandler, K., Shaykhiev, R., Kleemann, P., Klescz, F., Lohoff, M., Vogelmeier, C., and Bals, R. (2006) The anti-microbial peptide LL-37 inhibits the activation of dendritic cells by TLR ligands. *Int. Immunol. 18*, 1729−1736.
(41) Semple, F., Webb, S., Li, H. N., Patel, H. B., Perretti, M., Jackson, I. J., Gray, M., Davidson, D. J., and Dorin, J. R. (2010) Human beta-defensin 3 has immunosuppressive activity in vitro and in vivo. *Eur. J. Immunol. 40*, 1073−1078.
(42) Singer, D., Zauner, T., Genz, M., Hoffmann, R., and Zuchner, T. (2010) Synthesis of pathological and nonpathological human exon 1 huntingtin. *J. Pept. Sci. 16*, 358−363.
(43) Gausepohl, H., Pieles, U., and Frank, R. W. (1992) in *Peptides - Chemistry and Biology: Proceedings of the 12th American Peptide Symposium* (Smith, J. A. Rivier, J. E., Eds.) pp 523−524, ESCOM Science, Leiden.
(44) Zhu, X. T., Zhao, X., Burkholder, W. F., Gragerov, A., Ogata, C. M., Gottesman, M. E., and Hendrickson, W. A. (1996) Structural analysis of substrate binding by the molecular chaperone DnaK. *Science 272*, 1606−1614.
(45) Kabsch, W. (2010) XDS. *Acta Crystallogr., Sect. D: Biol. Crystallogr 66*, 125−132.
(46) Bailey, S. (1994) The Ccp4 suite - programs for protein crystallography. *Acta Crystallogr., Sect. D: Biol. Crystallogr. 50*, 760−763.
(47) Vagin, A., and Teplyakov, A. (1997) MOLREP: an automated program for molecular replacement. *J. Appl. Crystallogr. 30*, 1022−1025.
(48) Emsley, P., and Cowtan, K. (2004) Coot: model-building tools for molecular graphics. *Acta Crystallogr., Sect. D: Biol. Crystallogr. 60*, 2126−2132.
(49) Murshudov, G. N., Skubak, P., Lebedev, A. A., Pannu, N. S., Steiner, R. A., Nicholls, R. A., Winn, M. D., Long, F., and Vagin, A. A. (2011) REFMAC5 for the refinement of macromolecular crystal structures. *Acta Crystallogr., Sect. D: Biol. Crystallogr. 67*, 355−367.
(50) Mosmann, T. (1983) Rapid colorimetric assay for cellular growth and survival - application to proliferation and cyto-toxicity assays. *J. Immunol. Methods 65*, 55−63.
(51) Cook, J. A., and Mitchell, J. B. (1989) Viability measurements in mammalian-cell systems. *Anal. Biochem. 179*, 1−7.
(52) Gobbo, M., Benincasa, M., Bertoloni, G., Biondi, B., Dosselli, R., Papini, E., Reddi, E., Rocchi, R., Tavano, R., and Gennaro, R. (2009) Substitution of the arginine/leucine residues in apidaecin Ib with peptoid residues: Effect on antimicrobial activity, cellular uptake, and proteolytic degradation. *J. Med. Chem. 52*, 5197−5206.
(53) Gjedde, A. (1981) High-affinity and low-affinity transport of D-glucose from blood to brain. *J. Neurochem. 36*, 1463−1471.
(54) Triguero, D., Buciak, J., and Pardridge, W. M. (1990) Capillary depletion method for quantification of blood-brain-barrier transport of circulating peptides and plasma-proteins. *J. Neurochem. 54*, 1882−1888.
(55) Gutierrez, E. G., Banks, W. A., and Kastin, A. J. (1993) Murine tumor-necrosis-factor-alpha is transported from blood to brain in the mouse. *J. Neuroimmunol. 47*, 169−176.
(56) Frimodt-Moller, N., Knudsen, J. D., and Espersen, F. (1999) *Handbook of Animal Models of Infection*, Academic Press, London.